Full paper

Development of an Intelligent Chair Tool System Applying New Intelligent Pneumatic Actuators

Ahmad 'Athif Mohd Faudzi [a,b,*], **Koichi Suzumori** [a] **and Shuichi Wakimoto** [c]

[a] Graduate School of Natural Science and Technology, Okayama University, 3-1-1 Tsushima-naka, Okayama 700-8530, Japan

[b] Faculty of Electrical Engineering, Universiti Teknologi Malaysia, 81310 Johor Bahru, Malaysia

[c] Research Core for Interdisciplinary Sciences, Okayama University, 3-1-1 Tsushima-naka, Okayama 700-8530, Japan

Abstract

This paper develops an Intelligent Chair Tool (ICT) — a new chair-type human and machine interaction seating system powered by 36 intelligent pneumatic actuators. This tool can be used to facilitate investigation of chair shapes from spring and damping effects of seating and backrest surfaces. Each actuator used consists of five extensive elements of encoder, laser strip rod, pressure sensor, valves and PSoC microcontroller incorporated in a single device. By using the ICT, different shapes, spring and damping characteristics can be obtained to aid the design of chairs from the control inputs, i.e., position x, stiffness k_s and viscous coefficient c. Several control algorithms are presented to realize the communication and control system, and to obtain all data in real-time. The control methodology presented contains an inner force loop and an outer position loop implemented using a unified control system. The specification, development design and experimental evaluation of the ICT control system and actuator used are presented and discussed.
© Koninklijke Brill NV, Leiden and The Robotics Society of Japan, 2010

Keywords

Intelligent Chair Tool, seating system, intelligent pneumatic actuator, physical human machine interaction, control application in mechatronics.

1. Introduction

Chairs have been one of the important tools in human daily activities as the sitting position is considered the most frequent body posture in industrialized countries [1]. Undeniably, comfortable seating is an important issue in creating a mutual environment towards excellence in health and in daily works [2]. Various studies have been

---

[*] To whom correspondence should be addressed. E-mail: athif@act.sys.okayama-u.ac.jp

performed on postures and shapes of chairs. For instance, Holden *et al.* [3] used an adjustable seating rig to create the three-dimensional shape of a static lounge chair. Questionnaires were used to evaluate the comfort, but the study was just on chair shapes without considering other attributes. On the other hand, Yamazaki *et al.* presented an experimental chair with backrest and seats that made use of 10 and six actuator bars, respectively, to study suitable chair characteristics [4]. However, the damping parameter is not clearly defined and there are limitations of stiffness characteristics that have to be tuned mechanically. The backrest and seat unit also have a static value in a vertical line as the unit is connected in bar type. Other works that have been reported by Brienza *et al.* [5] applied a research tool that allows for control of surface shape using CASS — a computer-aided seating system based on force control feedbacks. Nevertheless, the study was done only on the seat surface and applied actuators using stepping motors, which largely depend on the drive circuits. Other works on chair studies and pressure distribution were contributed by other researchers [6–9].

The need for a research tool that allows control of a surface with simultaneous measurement of pressure distribution and finding suitable sitting postures that can help in chair development is presented in this paper. Development and experimental evaluation of an Intelligent Chair Tool (ICT) and its control system are discussed. The system are proposed as a spring–damping system by obtaining the spring and damping attributes using the pneumatic mechanical effect from intelligent actuators. Other research such as by Yoonkwon Hwang [10] also applies this system where he applied virtual spring–damping for a humanoid robot. Improved ergonomic shapes resulting from suitable damping and spring characteristics will position the lumbar curve perfectly and allow minimum back muscle activity [2, 11]. Three characteristics of shapes, spring and damping are proposed for the comfort of the users. These three characteristics are achieved using intelligent pneumatic cylinders as sensors and actuators for the system. As shown in Fig. 1, actuators and sensors will act as the interface between these two main components for input and output processes synchronously for human machine interaction. This physical human–machine interaction involves physical data information that is based on bilateral physical information exchange between the human and the machine (ICT). Other works such as active links with polyhedral and icosahedron shapes by Suzumori *et al.* also applied physical human–machine interaction for real-time multiple force-presentation interactions with a PC [12].

A pneumatic system is chosen because of the advantages of high power-to-weight ratio, lightweight, comparatively low cost, easier maintenance and having a simpler structure compared to other actuators [12–14]. A pneumatic actuator also has natural impedance with true mechanical compliance that does not exist in other actuators [15], which could present two main characteristics of stiffness and damping feedback with its systems. Previous work presents control algorithms and emulation experiments using a prototype cylinder [16] and structure details of the new developed actuators [17]. This present work is the extension of previous work
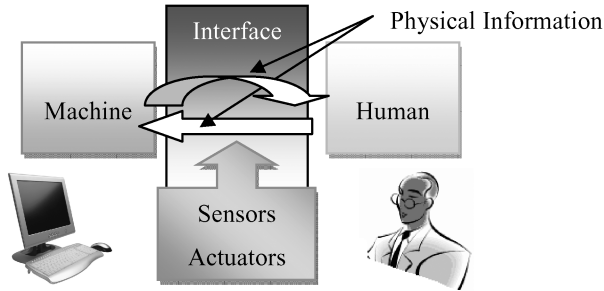
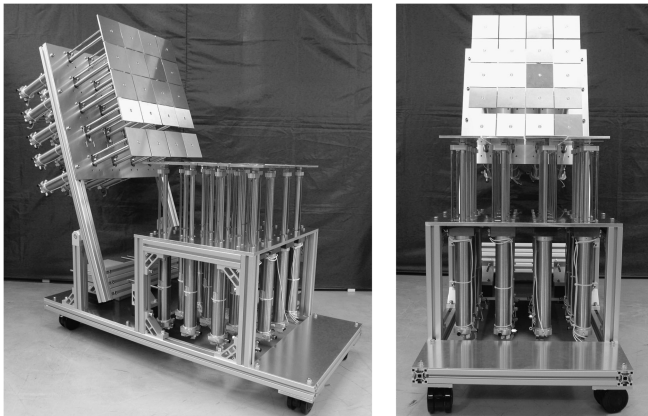**Figure 1.** Physical human–machine interaction.

Figure 2. ICT system.

to include the development of the ICT system applying the new intelligent actuators and experimental evaluation of its operation. The ICT application will have 36 links of intelligent actuators to receive physical information, and give feedback response of shape, spring and damping from the user dynamics as shown in Fig. 2. This paper mainly considers several algorithms, i.e., position, force, compliance and viscosity control, to test the functional ability of the intelligent actuator, and a combination of the algorithms realizes the spring and damping effects for the sitting experiments.

The remainder of this paper is organized as follows. Section 2 describes the ICT design and mechanism. Section 3 presents the development of a new intelligent actuator for the ICT. The experimental system and control algorithm is presented in Section 4. Experimental results of single intelligent actuators are presented in Section 5 and Section 6 discusses the operation of the ICT. Finally, Section 7 concludes with suggestions for future works.
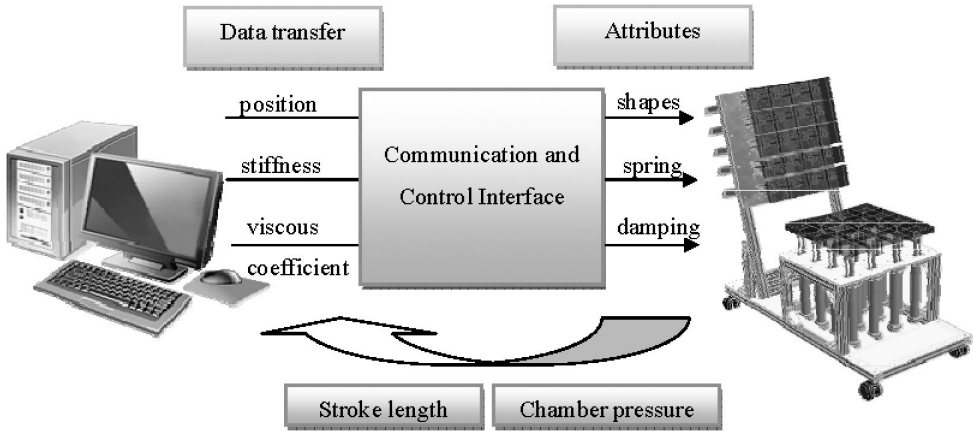
Figure 3. ICT overall system.

2. ICT Design and Mechanism

2.1. System Review

The ICT system involves three data sets as inputs from a PC that is *a priori* set as shown in Fig. 3. The three data sets are: position, stiffness and viscous coefficient that will be sent as control input to the ICT through the communication and control interface. Integration of 16 actuators on the seating panel and 20 actuators on the backrest receiving these data sets will give the chair the desired attributes of shape, spring and damping characteristics as controlled outputs of the system. Two feedback data sets of stroke length and chamber pressure from each actuator will be measured for further analysis.

   The communication and control interface are applied in an integrated manner such that only target data was sent from the PC and tasks are performed locally by each actuator. The states of each actuator are controlled locally using a PSoC microcontroller that has the ability of communication and control. This will give the system high reliability and intelligence to decide the output from the input given by the interaction of human weight and body shape.

2.2. Damping and Spring Characteristics

Damping and spring characteristics from the Voigt model are used where a viscous damper and purely elastic spring are connected in parallel as in Fig. 4 [18]. An ideal spring–damper system with spring constant k_s and viscous damper of damping coefficient c is subject to an oscillatory force:

$$F_s = -k_s x, \tag{1}$$

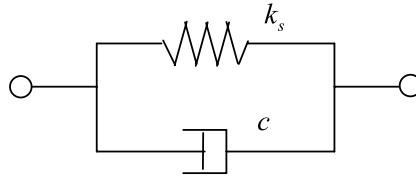and a damping force:

$$F_d = -cv = -c\dot{x}. \tag{2}$$

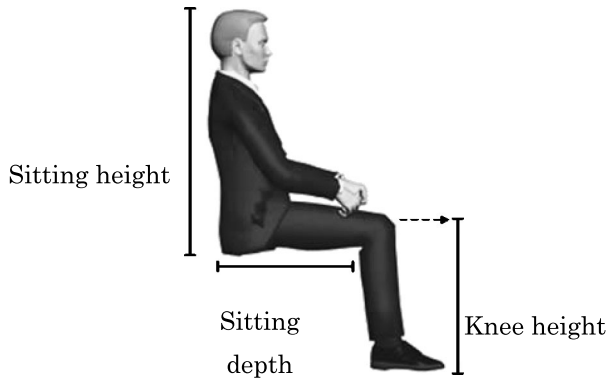**Figure 4.** Schematic representation of the Voigt model.

Figure 5. Common anthropometric measurements for the seated position [2].

From (1) and (2), the equation that relates spring and damping characteristics is given as:

$$F = -k_{\mathrm{s}}x - c\dot{x}, \tag{3}$$

where F, k_{s}, x, c and $\dot{x}$ are the force, stiffness, position, viscous coefficient and speed, respectively.

The actuator designed will realize these spring and damping characteristics with the mechanical effect from the pneumatic system for the ICT function.

2.3. Anthropometry Data and ICT Structure

In designing the ICT, anthropometry data for the seated position was taken from 30 Japanese students and compared with the Business and Institutional Furniture Manufacturer's Association (BIFMA) Standards to guide the overall structural design.

Therefore, data collection was done to study several dimensions on the System Integration Laboratory, Okayama University students. Data involving 23 male and two female subjects were measured. Five dimensions were taken, i.e., height, weight, seat height, seat depth and back seat height, as in Fig. 6.

The ICT is then designed using Autodesk Inventor CAD software — for size estimation and characteristics confirmation. Table 1 shows the size and characteristics of the ICT in comparison with BIFMA Standards [2].

Figure 6. Measurement process.

Table 1.
Comparison of the ICT characteristics with BIFMA [2] standards

Cylinder items	BIFMA Standard	ICT
Seat height (cm)	38.1–50.5	35–55
Seat depth (cm)	not less than 42.9	44–54
Seat width (cm)	not less than 45.7	46
Backrest height (cm)	more than 45	54–64
Backrest width (cm)	more than 36.1	43
Lumbar support (cm)	15.2–25.4	16–26
Backrest angle (deg)	90–115	90–125

2.4. ICT Parts

The structure of the ICT is made of aluminum pillars and aluminum plates. Two aluminum plates formed the base of seat and the backrest. On each of these plates was mounted 16 and 20 intelligent actuators for the seating and backrest panel, respectively. Each actuator is topped with rectangular aluminum disks of 100 mm × 100 mm to form the surface of each panel. Initially, the panel is not covered with any cloth or foam so that the stiffness k_s and viscous coefficient c from the material do not influence the experiments. After determining the suitable allowance for stiffness and damping, the plates will be covered with urethane rubber for a user-friendly seating surface.

The number of actuators on each panel depends on the assumptions of tactile sensitivity of the buttocks, thighs and back body [19], and coordination of the actuators. There are 10 main cylinders to support the user's weight as in Fig. 7. Therefore, a maximum of a 120-kg user can be supported by the ICT showing the ability of each cylinder to support a weight up to 12 kg [17]. Figure 8 shows the backrest panel adjusting mechanism to adjust the backrest angle. The ICT is able to adjust the angle of inclination in the range of 90–125° to achieve the desired inclination of the backrest angle. On the other hand, seating panel height can also be adjusted in the range of 35–55 cm.
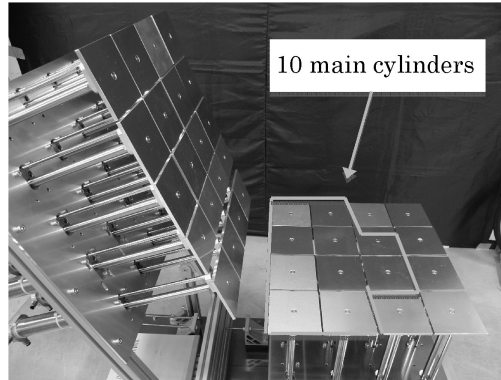
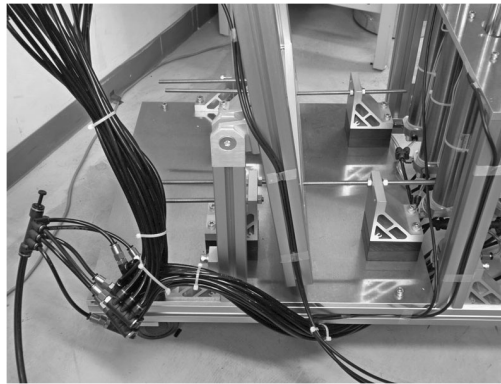**Figure 7.** Seating and backrest panels.

Figure 8. Backrest panel adjusting mechanism and air lines.

Figure 9 shows the installation of the intelligent actuator to the ICT with a simple communication line and air line. The communication line is connected serially from one actuator to another, whereas the air line is connected in parallel. Tires are attached for easy movement of the ICT.

3. Development of a New Intelligent Actuator for the ICT

3.1. Structure of a New Intelligent Actuator Design

A new intelligent actuator that combines software and hardware architectural design is developed. The cylinder is equipped with five elements, i.e., encoder, laser stripe rod, pressure sensor, valves and PSoC microcontroller, as shown in Fig. 10. Table 2 shows the specification comparison between the previous prototype cylinder and the newly developed intelligent actuator. The term 'intelligent' is used because the actuator has the ability to process data and give output based on the input response locally. Two types of sensors are applied: a micro optical encoder chip is used to

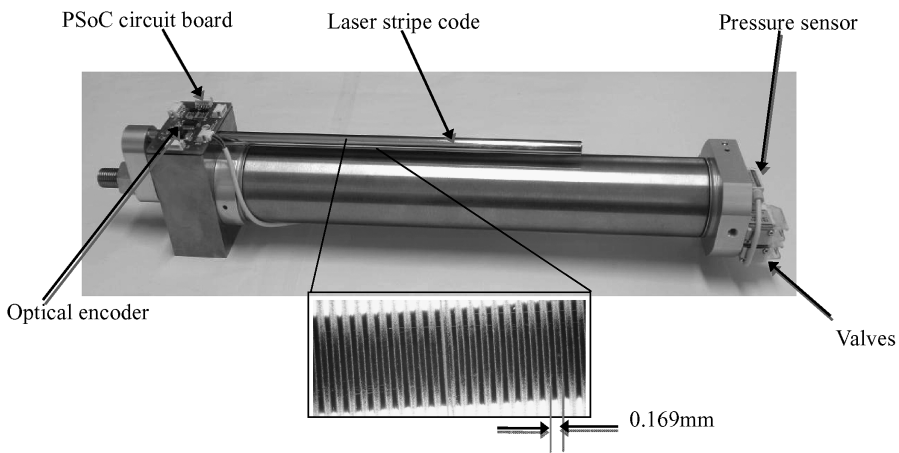**Figure 9.** Combination of intelligent actuators to form the ICT.

Figure 10. Intelligent actuator parts and zoomed laser strip code on the guide rod.

detect the cylinder rod position, whereas a pressure sensor is used to detect the chamber pressure reading.

For driving the actuator movements, two unit valves of two ports, two positions (2/2 valves) are used by manipulating pulse width modulation (PWM) cycles. The laser stripe codes were fabricated through a selective oxidation process by irradiating yttrium aluminum garnet (YAG) laser and enabling its motion detection through the encoder for determining the position value.

This actuator has also excellent communication ability where it can be controlled locally using only four wiring cables (two for VCC and GND; two for I^2C line) for real-time execution. This makes data transfer easier and faster for a system that uses many intelligent actuators such as the ICT applications. The control algorithms can be performed locally and in a distributed way, making it a novel intelligent actuator that can be applied to any other suitable application.

The main differences are the available elements on the cylinder and the overall actuator size. The installation of the laser strip rod on the guide rod also improves the sustainability of the actuator when installed separately from the cylinder rod.

Table 2.

Comparison of the previous prototype cylinder [11] and the new intelligent actuator

Cylinder items	Previous	New
Available elements	encoder and strip rod	encoder, strip rod, pressure sensor, PSoC board, valves
Length (mm)	133	388
Cylinder diameter (mm)	10	40
Rod diameter (mm)	3	16
Rod stroke (mm)	40	200
Laser strip pitch (mm)	0.338	0.169
Laser strip installation	together with cylinder rod	separated from piston rod, together with guide rod
Maximum force at 0.6 MPa (N)	8.5	120

The laser pitch also improved the position accuracy of 0.169 mm compared to the previous pitch of 0.338 mm. The new bigger actuator can of course drive a bigger force required for the ICT application of maximum 120 N at 0.6 MPa.

Figure 11 shows the schematic diagram of the intelligent actuator system that consists of several inputs and outputs. The input parts are the MEMS encoder and pressure reading. The encoder will read the laser stripe code on the guide rod shaft and send the signal to the counter module inside the PSoC to decide on the position of the cylinder stroke. A miniature pressure sensor will read the chamber pressure for feedback through an ADC module. The PSoC has the ability of embedding both digital and analog modules in a single chip, making the development process of the actuator communication and control easier. The output part of the system is the driven duty cycle from the PWM module to the valves and output signal from the I/O module to the LED. The I^{2}C module inside the PSoC was used for the communication between the intelligent actuator and communication board. The hardware design of the intelligent actuator and details of the parts used are presented in our previous report [17].

3.2. Operating Principle and Valve Operation of an Intelligent Actuator

The operating principle of the new intelligent pneumatic cylinder is shown in Fig. 12 where a simplified mechanical model is used. When pressure is applied to each chamber, the driving force that can be calculated as the output of external forces F_d is represented by:

$$F_d = P_2 A_2 - P_1 A_1 - F_r, \tag{4}$$

where F_d is the driving force, F_r is the friction force, P_1 and P_2 are pressures, and A_1 and A_2 are cross-sectional areas.

The above equation shows that the behavior of the cylinder can be controlled by manipulating the pressure in each chamber for right and left movements. In this research, an industrial pressure value of 0.6 MPa air supply is used. The method of
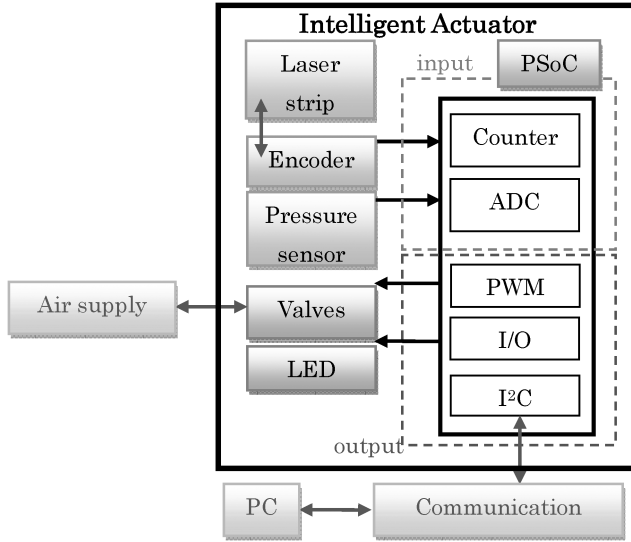
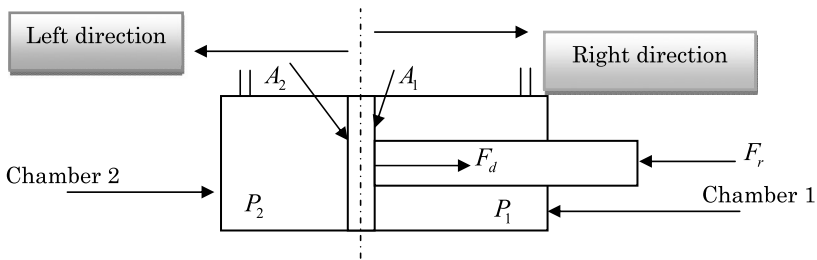**Figure 11.** Schematic diagram of the intelligent actuator system.

Figure 12. Principle of the intelligent actuator and its nomenclature.

controlling the actuator movements is by supplying constant air pressure to chamber 1 at 0.6 MPa (P_1) while regulating air inside chamber 2 from 0 to 0.6 MPa (P_2). Right and left movements depend on the algorithm to drive the valve using the PSoC PWM duty cycle in chamber 2. This method simplified the air system and can fulfill the ICT requirement of a maximum drive force of 120 N.

Friction force for the system can be divided into static and viscous friction as in (5). The mechanical friction inside the chamber is mainly caused by the sliding rubber seals that are used to prevent air leakage between chambers. The friction characteristics are shown in Fig. 13 where the static friction is around 10.8 N at 0.054 MPa and the viscous friction coefficient is 33.52 Ns/mm obtained from the steepness of the average line from the least-squares method. The frictional forces are:

$$F_r = F_{st} + c\dot{x}, \tag{5}$$

where F_{st} is the static friction, c is the viscous coefficient and $\dot{x}$ is the speed.
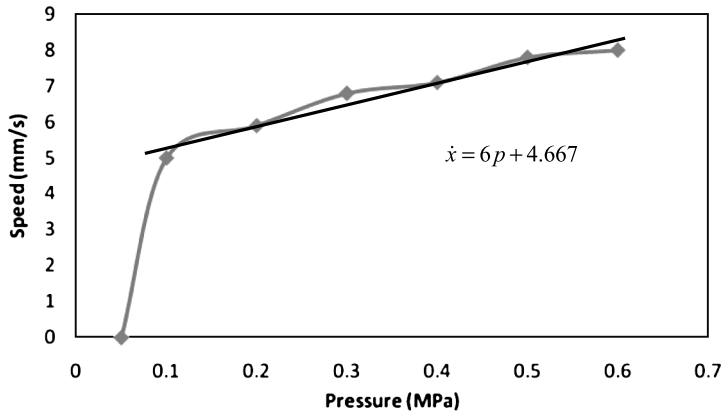
Figure 13. Friction characteristics from the rod stroke speed at equivalent air pressure.

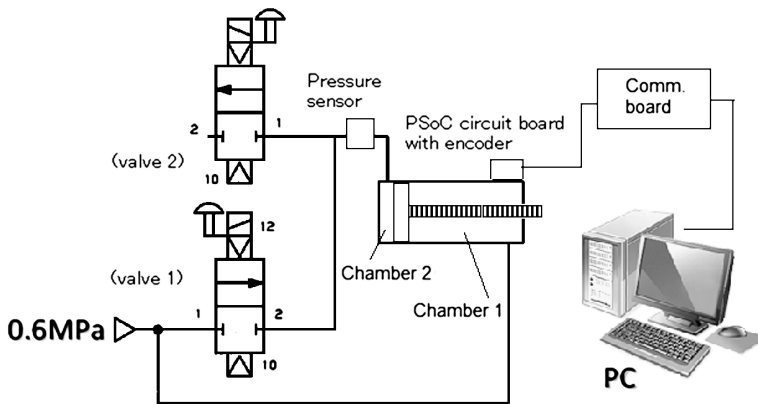In the figure: $\dot{x} = 6p + 4.667$

Figure 14. Valve operation for the intelligent actuator.

Two set of 2/2 valves are selected for minimizing the movements of actuator stroke when the actuator achieves the target position. This will reduce the valve operation where a normal on/off valve will always move to maintain a certain position. Figure 14 shows the schematic diagram for the intelligent actuator valve operation. Below are the possible movements of the cylinder that depend on the valve operation:

  (i) Valve 1 off; Valve 2 off — cylinder stops.
 (ii) Valve 1 off; Valve 2 on — cylinder moves right.
(iii) Valve 1 on; Valve 2 off — cylinder moves left.
 (iv) Valve 1 on; Valve 2 on — no operation.

By controlling only air inlet in chamber 2, the controlling mechanism is much easier to apply than controlling both chambers, thus reducing the number of valves used. Previous researchers [14, 20] had used the on/off solenoid valves for position control and were successful in addressing smooth actuator motion. However, they

Table 3.
Characteristics of the valves used in the intelligent actuator

Items	Sensor
Media	air
Operation type	internal pilot type
Operating pressure range (MPa)	0.2–0.7
Response time (ms)	6
Operating frequency (Hz)	20

applied multiple valves per cylinder, which increases the cost and makes the control approach more complex.

Table 3 shows the parameters of the valves used. The valve operating frequency of 20 Hz was used in the calculation of the PWM duty cycle to control the actuator movements.

4. Experimental System and Control Algorithm

4.1. Experimental System

In this study, the experimental evaluation is divided into two parts. The first part is the single actuator experiments that are detailed in Fig. 15. The second part is the sitting experiment evaluation using the ICT. The overall experimental setup in this study is shown in Fig. 16. It consists of a PC (Pentium 4, XP Operating System), power supply (24 V 14 A), communication board (USB, SPI and I^2C protocol), single-actuator experimental setup, ICT and air supply line.

For the single-actuator experiment, a force gauge is used for recording the force value from the pushing of the cylinder stroke in compliance and viscosity control experimental evaluation. Hence, the cylinder stroke is connected to a force gauge using a designed connector. Then the force gauge is fixed to a motor plane that can move forwards and backwards depending on the stepping motor movements. The position of the force gauge is kept aligned with the actuator stroke to eliminate any additional force.

4.2. Communication and Air System

The communication system for the ICT is divided into three main protocols — universal serial bus (USB), serial peripheral interface (SPI) and inter-integrated circuit (I^2C) using PSoC chips. Figure 17 shows the system configuration diagram of the ICT communication system. The communication protocol between the PC and communication board applies the USB protocol. Then, the SPI protocol is used between master and subcircuits. Finally, the I^2C protocol is performed between subcircuits to the ICT system. The I^2C protocol only needs two connectors, which are the serial clock line (SCL) and serial data line (SDA), thus reducing the amount of wiring for the system.
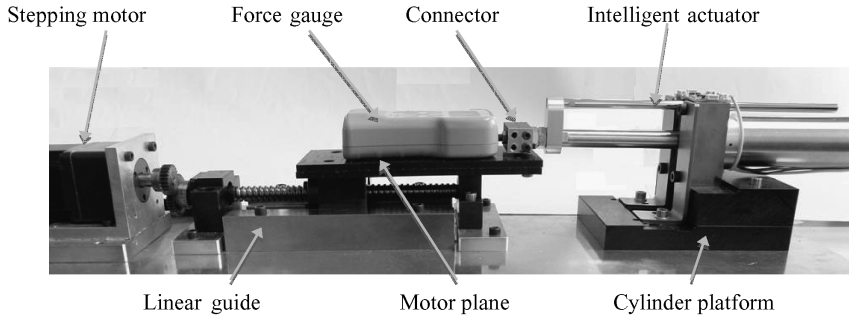
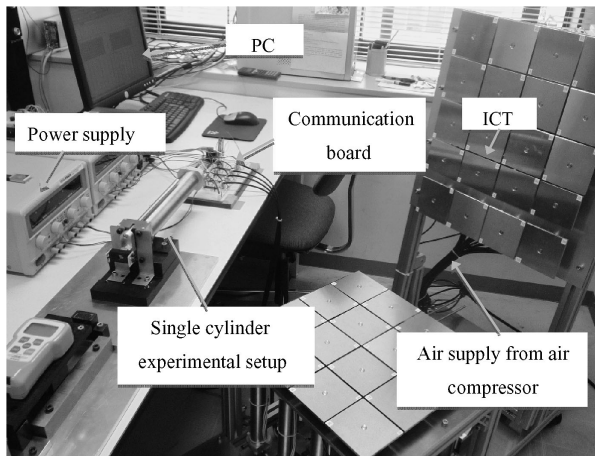**Figure 15.** Experimental setup for the single actuator.

Figure 16. Overall experimental setup.

In detail, the main circuit consists of USB and SPI Master modules realizing the USB protocol from the PC. From the main circuit, the SPI protocol is realized between four chips on the subcircuit. Each chip contains SPI Slave and I^{2}C Master modules. Then, the I^{2}C protocol is used to communicate with the actuator in serial on the ICT. The I^{2}C protocol communicates in 8, 8.10 and 10 links in serial and to make a combination of all 36 links of actuators. This methodology allows distributed control from the PC where control functions are perform locally in each actuator, thus giving this system high reliability of data transfer and control in real-time.

For the air system, the air compressor sends the air supply to the system. An air regulator is used for regulating the required value for the system of stable 0.6 Mpa air pressure. The air is then supplied to the actuator and driven by the PWM duty cycle to control the valve movement.

4.3. Control Algorithms

The control algorithm for the ICT was designed using a unified control system inside the PSoC on each actuator. Initially, the actuator was tested experimentally for
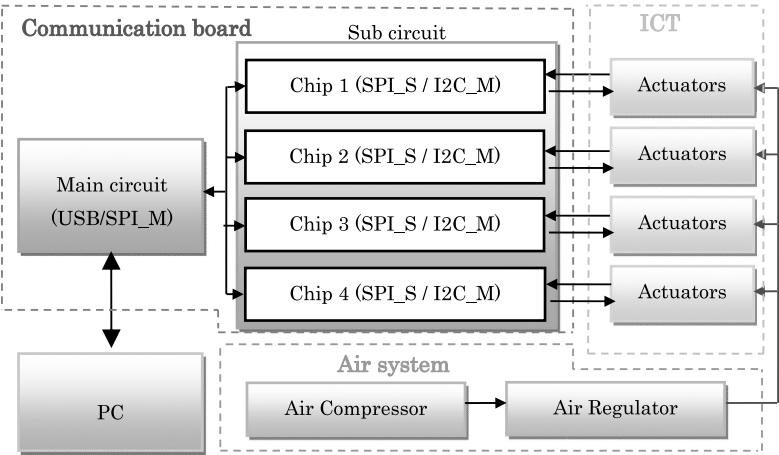
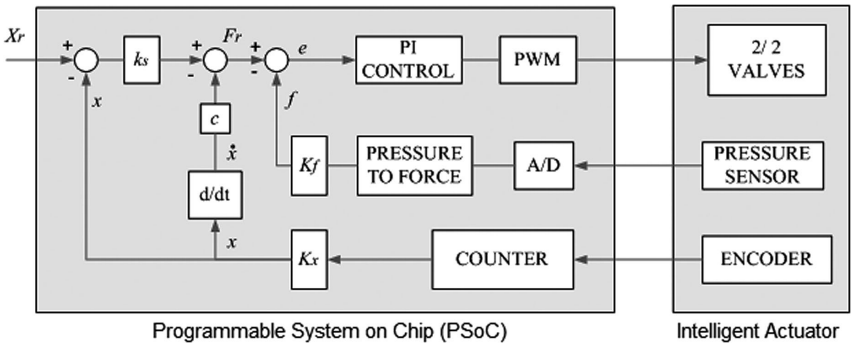**Figure 17.** System configuration diagram of the ICT communication system.

Figure 18. Unified control system block diagram.

functional ability using several control approaches, i.e., position, force, compliance and viscosity. Figure 18 shows the control block diagram using (3) and Table 4 details the parameters for each control algorithm selected to perform the control approach. The block diagram contains an inner loop to control force by receiving chamber pressure feedback, while an outer loop of position control for tracking the desired position and commands desired force to the inner loop. A PI controller is used in the force control loop to nullify the nonlinearity arising from the compressibility of air. Using the PWM module in the PSoC it is possible to drive the on/off valve easily to achieve the control objectives for each control approach.

In Table 4, there are four parameters to be selected for each control algorithms — viscous coefficient, stiffness, force and position parameters. These parameters can be easily selected for the desired control approach. As an example, for compliance control, c is set to zero and k_s is changed to observe the spring effect. In viscosity control, the value of k_s is set to zero and c is changed to observe the damping effect.

Table 4.
Specification of parameter settings for experiments

Experiments	c (viscous coefficient parameter; Ns/mm)	k_s (stiffness parameter; N/mm)	K_f (force parameter)	K_x (position parameter)
Position control	0	1	0	1
Force control	0	0	1	0
Compliance control	0	0.5, 1, 2	1	1
Viscosity control	1, 2, 3	0	1	1
Sitting experiment	0.2, 0.5, 1	0.5, 1, 3, 6	1	1

After confirming the workability of each control, the control algorithm to realize both spring and damping function for the ICT was done using the same block diagram by selecting all parameters. Through the unified control system, all experiments can be carried out easily by selecting the parameters needed from the PC and the algorithms are done locally using the PSoC. The communication ability and local control functions provide delicate and high performance of the actuator motions.

5. Experimental Results of a Single Intelligent Actuator

Towards realizing the operation of the ICT, four control algorithms are investigated using the developed intelligent actuator. The experimental studies are position, force, compliance and viscosity control. This study was done to evaluate the working ability of the intelligent actuator to perform the control algorithm and achieve the control objectives.

5.1. Position Control

For position control, the target position is given from PC. The error between the readings from the encoder is calculated by $e = X_r - x$, where X_r and x are position reference and current position, respectively. PI control was used with a suitable gain value to drive the valve using PWM to achieve the target cylinder position. Figures 19 and 20 show the experimental results of a sine wave and step response position tracking.

PI control shows great performance during sine wave tracking and step response with 0.169 mm position accuracy. Position control using an intelligent actuator is also possible for other positioning motion such as a ramp and S-curve as well as its good contribution towards disturbance rejection. Using position control, the target position of the actuators on the ICT is achieved to form different shapes of the chair structure.
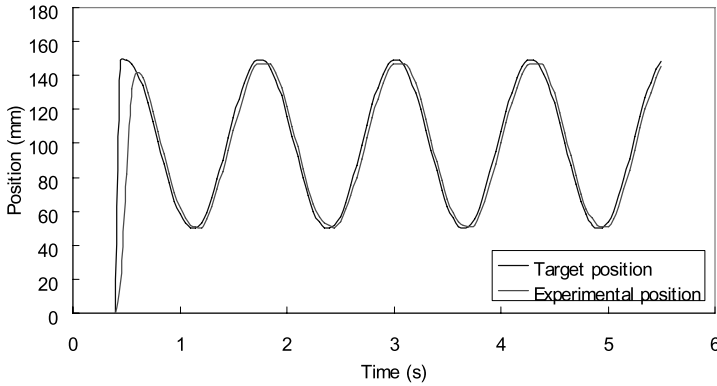
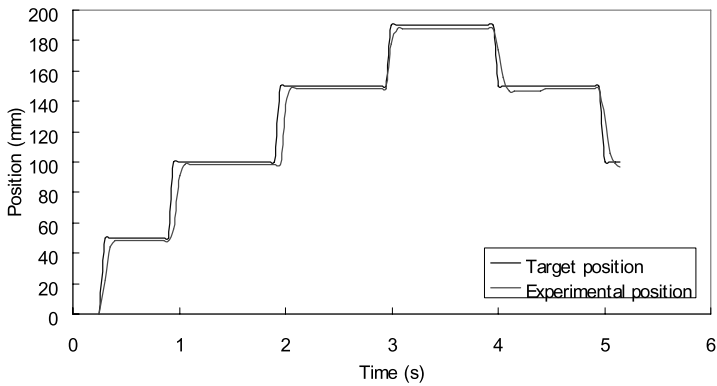**Figure 19.** Sine wave tracking using PI control.

Figure 20. Step response tracking using PI control.

5.2. Force Control

In this experiment, a force gauge is used to verify the output force from the actuator stroke. The experimental setup is as in Fig. 15, where the force gauge position is kept static with a distance between the initial position of the actuator rod of (50 mm). During the experiment, the actuator stroke extends and touches the force gauge at different force values depending on the target force.

The target force is given from the PC and the response of the output force is shown in Fig. 21. Some of the error observed is due to mechanical friction. However, the small error value is acceptable in human and machine interaction. In the system, the nonlinear characteristic does exist; however, the value is small compared to a rubber actuator. The actuator driving force mainly depends on the supplied pressure value and the cross-sectional area but does not depend on the actuator's rod position. This study is performed to confirm the inner loop response of the force loop towards the compliance, viscosity and sitting experiments.
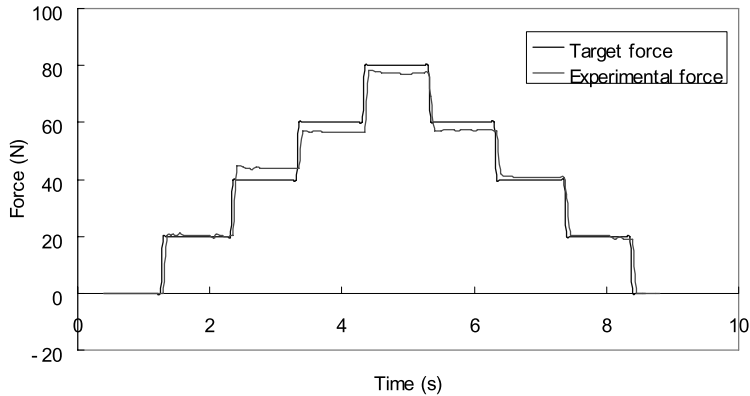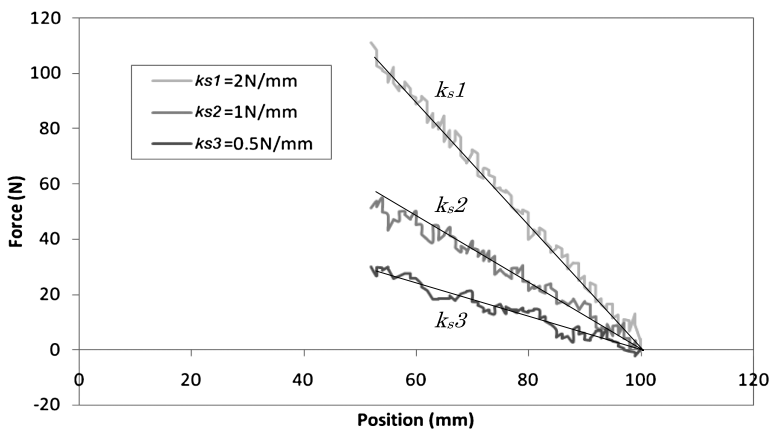
Figure 21. Experimental results of force tracking.

Figure 22. Experimental results of compliance control.

5.3. Compliance Control

In this experiment, the target position was set to the origin position (100 mm) by using the experimental setup as in Fig. 15. The motor plane was moved by a stepping motor in the backwards direction (100 to 53 mm) for studying the pushing force when changing the stiffness k_s to imitate the real sitting position of the ICT. Three different k_s inputs of 2, 1.5 and 0.5 N/mm were input from the PC, and the experimental results are given in Fig. 22.

From the results, feedback force from the actuator gives a positive force; however, the k_s slope is negative. This is because in (3), the slope characteristic is negative but the k_s value itself is positive. Figure 22 also shows bigger k_s values give a steeper feedback force while a large position error (from 100 mm) increases the force value. The experimental results show that the stiffness parameter was successfully applied to the intelligent actuator and the spring effect can be identified. The experimental k_s data are identical with the input data with minimum errors due

Table 5.
Comparison of experimental and theoretical data for compliance control

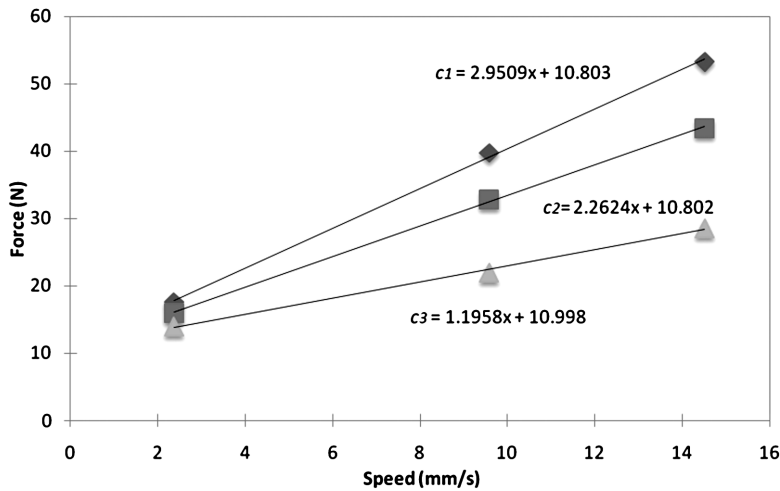| Compliance parameter	Cylinder experiment (N/mm)	Theoretical data (N/mm)
k_s1	0.558	0.50
k_s2	1.008	1.00
k_s3	2.096	2.00

Figure 23. Experimental results of viscosity control.

to the hardware friction inside the cylinder. Table 5 shows the comparison of the exerimental data and input data.

5.4. Viscosity Control

For the viscosity experiment, the speed of the cylinder stroke depends on the movements of the stepping motor that can be controlled by setting the motor frequency. In this experiment, the motor speed is adjusted to three different speeds; 2.4, 9.6 and 14.3 mm/s. Then, for each speed, three values of viscous coefficient c are: 1.0, 2.0 and 3.0 Ns/mm. The results are shown in Fig. 23.

From the results, the force data gives a linear response from the motor speed and the experimental c values are identical with the input given. Figure 23 shows the speed movement affects the feedback force and a bigger c value will also give a larger force feedback. Table 6 shows the comparison of the experimental data and input data with some minimum errors. This error occurs because of the nonlinearities that arise from the frictional force. This can be identified from the crossing point at speed 0 mm/s, where for all tested c values the force is around 10.8 N. This frictional force over the overall forces of 120 N has less than 10% error and is acceptable for the ICT system. The experimental results show that the viscous

Table 6.
Comparison of experimental and theoretical data for viscosity control

Viscous coefficient parameter	Cylinder experiment (Ns/mm)	Input data (Ns/mm)
c_1	1.196	1.00
c_2	2.262	2.00
c_3	2.951	3.00

Figure 24. ICT seating test for different weights of User A (80 kg), User B (60 kg) and User C (52 kg).

coefficient parameter was successfully applied to the intelligent actuator and the damping effect can be identified.

6. Operation of the ICT

6.1. Experimental Evaluation of Real-Time Sitting Experiments

Sitting experiments of the ICT system to study the shape, spring and damping characteristics of chairs were carried out. In this experiment, three users with different weights sit on the ICT, and the ICT, will give a feedback response from the actuators depending on the stiffness k_s and viscous coefficient c parameters input from PC. Figure 24 shows Users A, B and C with different weights of 80, 60 and 52 kg, respectively. The shape and stiffness studies involve Users A and B, while the viscous coefficient study was carried out with User C.

6.2. Shape Study

Using the ICT, various chair shapes can be obtained easily using the position control in the PSoC. Two different shapes are shown in Fig. 25. The left figure shows a flat surface of the backrest and a seating panel with 95° inclination between each panel. On the other hand, right figure shows a non-flat surface with 105° inclination between each panel. In Fig. 25, the angle of the platform is not changed, the differ-
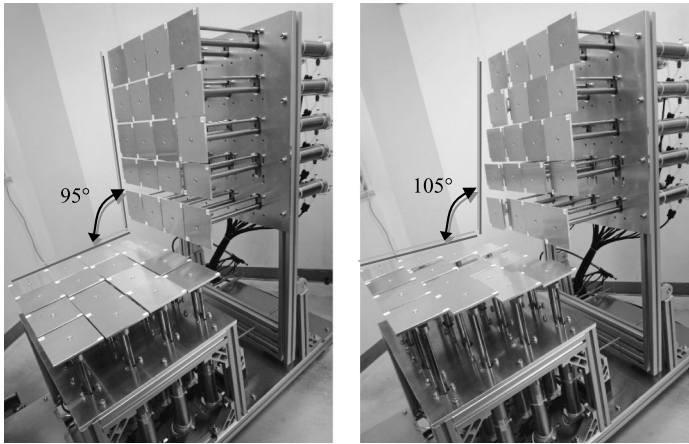
Figure 25. Different shapes of the ICT applied using position control.

Figure 26. Non-flat seating surface with inclination.

ent angles are created by adjusting the positions of each of the actuators. The flat surface chair shape was used for ICT sitting experimental evaluation for stiffness and viscous coefficient studies.

Figure 26 shows a zoomed picture of the non-flat seating surface. The position of the actuators form curves for different shapes of the surface controlled by the PSoC. For the viscous coefficient study, the characteristics of actuators 1, 2, 3 and 4 of the seating panel in Fig. 26 are discussed.

6.3. Stiffness Study

Both Users A and B sit on the ICT with position x, stiffness k_s and viscous coefficient c that are set *a priori* from the PC. Figures 27 and 28 show the responses for four values of stiffness: two for seating panel, $k_{s1} = 6$ N/mm, $k_{s2} = 2$ N/mm, and two for backrest, $k_{s3} = 1$ N/mm, $k_{s4} = 0.5$ N/mm, at a constant value of viscous coefficient $c = 0.2$ Ns/mm. The initial position in this experiment for the backrest is $x_1 = 180$ mm and $x_2 = 100$ mm for the seating panel. The angle between the seating and backrest panels is 95°.
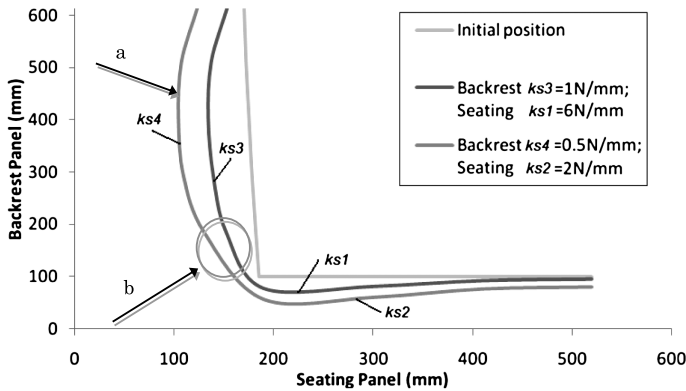
Figure 27. Sitting experiment with different stiffness values for User A (80 kg).
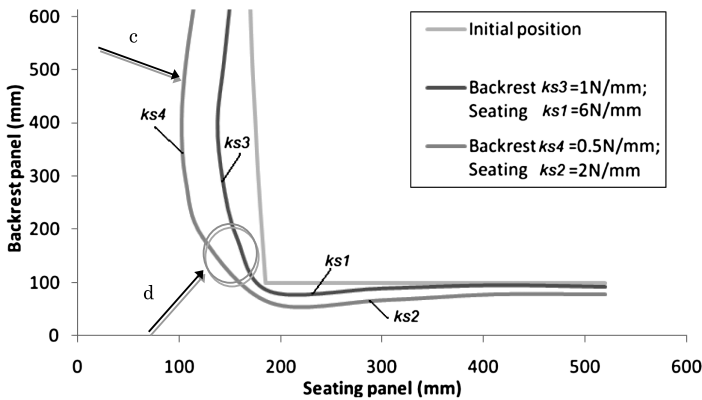

Figure 28. Sitting experiment with different stiffness values for User B (60 kg).

From Figs 27 and 28, we can study the different appropriate shapes of the chair surface for Users A and B body back shape at different stiffness values but constant viscous coefficient. User A has a curved body back (a) while User B has a straighter back (c). The lumbar curve for each user can also be identified at (b) and (d). The comparison of stiffness values at the seating panel, $k_{s1} = 6$ N/mm, $k_{s2} = 2$ N/mm for users A and B is detailed in Fig. 29 at constant $c = 0.2$ Ns/mm. The initial seating height is set at $x_2 = 100$ mm.

From Fig. 29, we can see that the bigger k_s value ($k_{s1} = 6$ N/mm) will give a stiffer spring response. However, User A, who is heavier than User B, has a bigger displacement when sitting at $k_{s2} = 2$ N/mm compared to User B because of less stiff spring effects.

6.4. Viscous Coefficient Study

The study of the damping effect is focused on the seating panel for actuators 1, 2, 3 and 4 as shown in Fig. 26. User C, 52 kg in weight, sits on the ICT with changing values of viscous coefficient $c_1 = 1$ Ns/mm and $c_2 = 0.5$ Ns/mm. The stiffness
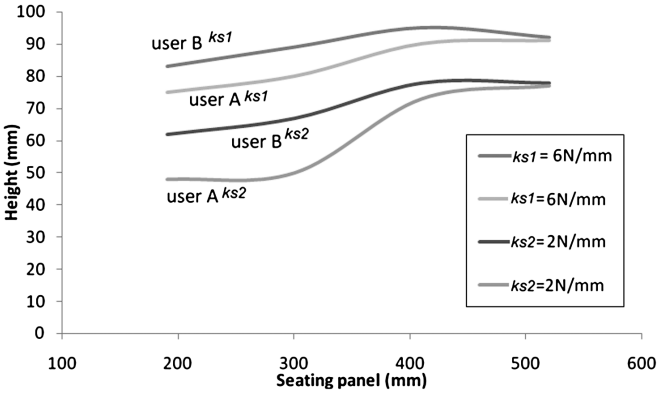
Figure 29. Comparison of stiffness values at the seating panel for Users A and B.

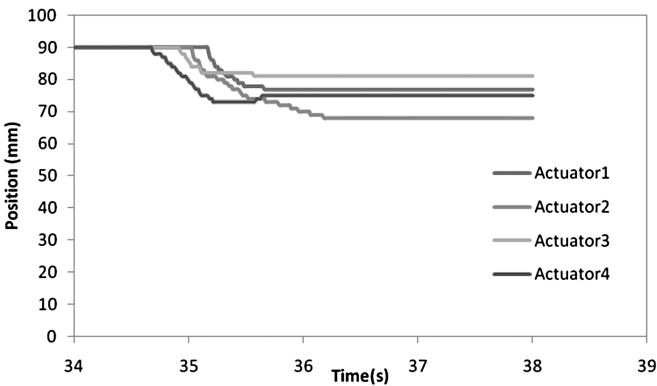**Figure 30.** Viscous coefficient $c = 1$ Ns/mm for the seating panel for User C.

parameter is kept constant at $k_s = 3$ N/mm. Figures 30 and 31 show the responses of the seating panel when the initial seating height is set at $x_3 = 90$ mm.

From Figs 30 and 31, when the viscous coefficient parameter c was changed, the actuator responded with the weight of User C. Figure 30 shows the response with $c_1 = 1$ Ns/mm that supports the user weight better compared to smaller c, $c_2 = 0.5$ Ns/mm, by giving the feedback force from the actuator. This shows that c_1 and c_2 give over-damping and under-damping characteristics, respectively. Actuators 1, 2 and 3 have the same settling position since the k_s value is set constant in both experiments. However, actuator 4 gives different settling positions because of different sitting postures and force distributions during the experiment.

The results show that the ICT can be applied successfully for under-damp and over-damp characteristics that are stable and suit the mass damping spring system. This is confirmed with the damping ratio value ζ, which can be calculated from (6)
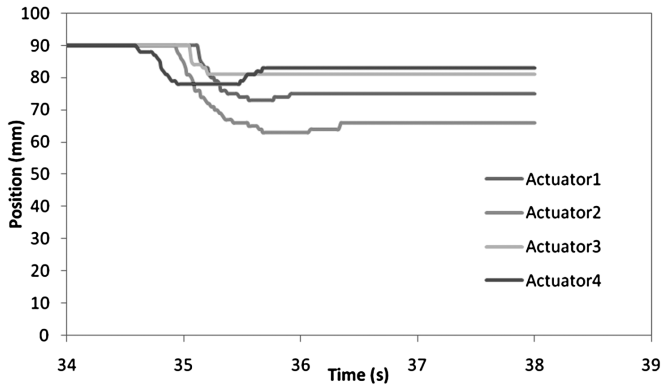
Figure 31. Viscous coefficient $c = 0.5$ Ns/mm for the seating panel for User C.

Table 7.
System characteristics in response to k_s and c

c (viscous coefficient; Ns/mm)	k_s (stiffness; N/mm)	ζ (damping ratio)	System characteristics
1	3	1.266	over-damping
0.5	3	0.633	under-damping

for the two different conditions of different values of c used in experiments. Table 7 shows the system characteristics in respond to k_s and c value calculated from:

$$\zeta = \frac{c}{2\sqrt{km}}. \tag{6}$$

Towards the real ICT function, the optimal damping and spring characteristics that suit the human comfort and ergonomics factor can be determined after iterations of trial-and-error experiment.

7. Conclusions

A new application of chair-type human–machine interaction using the ICT was presented. The developed ICT consists of 36 intelligent actuators with several hardware structures incorporated in a single device. The actuator actualizes local control of several algorithms for single-actuator and ICT sitting experiments. The effectiveness of all controllers is successfully verified using an experimental approach with input data from a PC. The stiffness parameter k_s from compliance control gives mechanical spring attributes, while viscous coefficient c from viscosity control gives mechanical damping effects.

The ICT sitting experiment shows the success of the system to respond to different users with different k_s and c parameter settings. The ICT could give various

chair shapes by changing the actuator positions, giving various spring characteristics from the stiffness parameter k_s and also giving different damper characteristics by manipulating the viscous coefficient c. The ICT system agrees with both under-damping and over-damping confirmed with the damping ratio calculated. The ICT sitting experiment evaluates both spring and damping effects to obtain the shapes of chairs for seating and backrest panels.

Further works involve a psychophysics study in selecting the best parameter of k_s and c so that the data could be used in designing ergonomically shaped chairs with certain stiffness and viscous coefficient values.

References

1. E. Grandjean and W. Hünting, Ergonomics of posture — review of various problems of standing and sitting posture, *Appl. Ergonom.* **8**, 135–140 (1977).
2. S. Openshaw and E. Taylor, *Ergonomics and Design: A Reference Guide*. Allsteel, Muscatine, IA (2006).
3. J. M. Holden and G. Fernie, Specifications for a mass producible static lounge chair for elderly, *Appl. Ergonom.* **20**, 39–45 (1989).
4. N. Yamazaki, T. Sasaki and J. Aizawa, Development of cushion-adjustable chair for analyzing individual sitting condition, *Hum. Eng.* **33**, 211–218 (1997). (In Japanese).
5. D. M. Brienza, R. M. Inigo, K.-C. Chung and C. E. Brubaker, Seat support surface optimization using force feedback, *IEEE Trans. Biomed. Eng.* **40**, 95–101 (1993).
6. M. Lengsfeld, A. Frank, D. L. van Deursen and P. Griss, Lumbar spine curvature during office chair sitting, *Med. Eng. Phys.* **22**, 665–669 (2000).
7. R. H. M. Goosen and C. J. Snijders, Design criteria for the reduction of shear forces in beds and seats, *J. Biomechan.* **28**, 225–230 (1995).
8. S. Matsumoto, H. Kawakami and Y. Uchimura, Experimental studies of chair design by multivariate analysis, *Eng. Faculty Kinki Univ. Kyushu Univ. Res. Rep.* **23**, 47–56 (1994) (In Japanese).
9. R. H. M. Goosen, C. J. Snijders, G. A. Hoek van Dijke and A. H. den Ouden, A new instrument for the measurement of forces on beds and seats, *J. Biomed. Eng.* **15**, 409–412 (1993).
10. Y. Hwang, E. Inohira, A. Konno and M. Uchiyama, An order *n* dynamic simulator for a humanoid robot with virtual spring–damper contact model, in: *Proc. Int. Conf. Robotics and Automation,* Taipei, pp. 31–36 (2003).
11. R. Lueder, *Ergonomics of Sitting and Seating*. Humanics Ergosystems, Encino, CA (2004).

12. J. Ochi, K. Suzumori, J. Tanaka and T. Kanda, Development of active links for physical man–machine interaction, *J. Robotics Mechatron.* **17**, 293–301 (2005).

13. I. L. Krivits and G. V. Krejnin, *Pneumatic Actuating Systems for Automatic Equipment Structure and Design*. CRC Press, Boca Raton, FL (2006).

14. S. Chillari, S. Guccionne and G. Muscato, An experimental comparison between several pneumatic position control methods, in: *Proc. 40th IEEE Conf. on Decision and Control*, Orlando, FL, pp. 1168–1173 (2001).

15. Y. Zhu and E. J. Barth, Impedance control of a pneumatic actuator for contact tasks, in: *Proc. IEEE Int. Conf. on Robotics and Automation*, Barcelona, pp. 987–992 (2005).

16. A. A. M. Faudzi, K. Suzumori and S. Wakimoto, Development of an intelligent pneumatic cylinder for distributed physical human–machine interaction, *Adv. Robotics* **23**, 203–225 (2009).

17. A. A. M. Faudzi, K. Suzumori and S. Wakimoto, Design and control of new intelligent pneumatic actuator for intelligent chair tool application, in: *Proc. IEEE/ASME, Int. Conf. on Advanced Intelligent Mechatronics*, Singapore, pp. 1909–1914 (2009).

18. M. Meyers and K. Chawla, Section 13.10, in: *Mechanical Behaviors of Materials*, pp. 570–580. Prentice Hall, Englewood Cliffs, NJ (1999).

19. S. Weinstein, Intensive and extensive aspects of tactile sensitivity as a function of body part, sex and literality, in: *The Skin Senses*, pp. 195–222. Thomas, Springfield, IL (1968).

20. R. B. Van Varsevald and G. M. Bone, Accurate position control of a pneumatic actuator using on/off solenoid valves, *IEEE/ASME Trans. Mechatron.* **2**, 195–204 (1997).

About the Authors

Ahmad 'Athif Mohd Faudzi received the BE degree in Computer Engineering and the ME degree in Mechatronics and Automatic Control Engineering from Universiti Teknologi Malaysia (UTM), in 2004 and 2006, respectively. He has been a Lecturer in the Department of Mechatronics and Robotics, Faculty of Electrical Engineering, UTM, since 2006. In 2007, he furthered his PhD in the Department of System Engineering, Division of Industrial Innovation Sciences, Okayama University, Japan. His current research interests include actuators, physical human–machine interaction, mechatronics and automatic control. He is a Member of the Institution of Engineers, Malaysia, the Institute of Electrical and Electronics Engineers, and the Japan Society of Mechanical Engineers.

Koichi Suzumori received the BS, MS and PhD degrees in Mechanical Engineering from Yokohama University, Japan, in 1982, 1984 and 1990, respectively. He worked for Toshiba R&D Center, from 1984 to 2001, and also worked for Micromachine Center, Tokyo, from 1999 to 2001. He has been a Professor of the Department of System Engineering, Division of Industrial Innovation Sciences, Okayama University, Japan, since 2001. He is mainly engaged in the research fields of new actuators and their applications. He has received many awards such as the JSME Medal for Outstanding Paper in 1999, RSJ Best Paper Award, in 2000, and JSAEM Best Book Award, in 2006. He is a Fellow Member of the Japan Society of Mechanical Engineers.
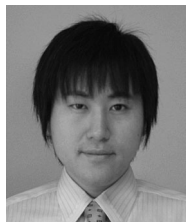
Shuichi Wakimoto received the BE, ME and DE degrees from Okayama University, Japan, in 2002, 2004 and 2007, respectively. He was a Research Fellow of the Japan Society for the Promotion of Science, from 2004 to 2007. Since 2007, he has been an Assistant Professor at the Graduate School of Natural Science and Technology, Okayama University, Japan. His research interests are flexible sensors and actuators. He is a member of the Japan Society of Mechanical Engineers and the Robotics Society of Japan.